Journal of Applied Physics

# Effect of electron–electron interaction on magnitude of quantum oscillations of dissipative resistance in magnetic fields

Cite as: J. Appl. Phys. **132**, 234302 (2022); https://doi.org/10.1063/5.0127286
Submitted: 20 September 2022 • Accepted: 26 November 2022 • Published Online: 15 December 2022

Sara Abedi, Sergey Vitkalov, A. A. Bykov, et al.





AIP Publishing

Journal of Applied Physics ARTICLE scitation.org/journal/jap

# Effect of electron–electron interaction on magnitude of quantum oscillations of dissipative resistance in magnetic fields

Cite as: J. Appl. Phys. **132**, 234302 (2022); doi: 10.1063/5.0127286
Submitted: 20 September 2022 · Accepted: 26 November 2022 ·
Published Online: 15 December 2022



Sara Abedi,[1] Sergey Vitkalov,[1,a)] A. A. Bykov,[2] and A. K. Bakarov[2]

## AFFILIATIONS

[1]Physics Department, City College of the City University of New York, New York, New York 10031, USA
[2]Rzhanov Institute of Semiconductor Physics, Siberian Branch, Russian Academy of Sciences, Novosibirsk 630090, Russia

[a)]**Author to whom correspondence should be addressed:** svitkalov@ccny.cuny.edu

## ABSTRACT

Magneto-intersubband resistance oscillations (MISOs) of highly mobile 2D electrons in symmetric GaAs quantum wells with two populated subbands are studied in magnetic fields $\mathbf{B} = (B_\perp, B_\parallel)$ tilted from the normal to the 2D electron layer at different temperatures $T$. The in-plane component ($B_\parallel$) of the field $\mathbf{B}$ induces magnetic entanglement between subbands, leading to beating in oscillating density of states (DOS) and to MISO suppression. Model of the MISO suppression is proposed. Within the model, a comparison of MISO amplitude in the entangled and disentangled ($B_\parallel = 0$) 2D systems yields both difference frequency of DOS oscillations, $df$, and strength of the electron–electron interaction, described by parameter $\varepsilon_F^*$, in the 2D system. These properties are analyzed using two methods, yielding consistent but not identical results for both $df$ and $\varepsilon_F^*$. The analysis reveals an additional angular dependent factor of MISO suppression. The factor is related to spin splitting of quantum levels in magnetic fields.



## I. INTRODUCTION

The orbital quantization of electron trajectories and spectrum in magnetic fields significantly affects the electron transport in condensed materials.[1–3] Shubnikov–de Haas (SdH) resistance oscillations[1] and quantum Hall effect (QHE)[4] are remarkable effects of the orbital quantization. These effects occur at a temperature, $T$, which is less than the cyclotron energy, $\Delta_c = \hbar\omega_c$, separating Landau levels. Here, $\omega_c$ is the cyclotron frequency. At high temperatures, $kT > \hbar\omega_c$, both SdH oscillations and QHE are absent due to spectral averaging of the oscillating density of states (DOS) in the energy interval, $\delta\varepsilon \approx kT$, in the vicinity of Fermi energy, $\varepsilon_F$.

At high temperatures, $kT > \hbar\omega_c$, electron systems with multiple populated subbands continue to exhibit quantum resistance oscillations.[5–10] These magneto-inter-subband oscillations (MISOs) of the resistance are due to an alignment between Landau levels from different subbands $i$ and $j$ with corresponding energies $E_i$ and $E_j$ at the bottom of the subbands. Resistance maxima occur at magnetic fields in which the gap between the bottoms of the subbands, $\Delta_{ij} = E_i - E_j$, is a multiple of the Landau level spacing: $\Delta_{ij} = k \cdot \hbar\omega_c$, where $k$ is an integer.[11–15] At this condition, Landau levels of two subbands overlap, and the electron elastic scattering on impurities is enhanced due to the possibility of electron transitions between the overlapped quantum levels of $i$th and $j$th subbands. At magnetic fields corresponding to the condition $\Delta_{ij} = (k + 1/2) \cdot \hbar\omega_c$, the inter-subband electron scattering is suppressed since the quantum levels of two subbands are misaligned. The spectral overlap between two subbands oscillates with the magnetic field and leads to MISO, which are periodic in the inverse magnetic field.

Recently, we have studied transport properties of high quality GaAs quantum wells with two populated subbands in tilted magnetic fields.[16,17] We have found a strong reduction of the MISO amplitude with the in-plane magnetic field[16] and the temperature.[17]

The effect was studied in a broad range of angles $\theta$ between the magnetic field, $\mathbf{B}$, and the normal to the 2D layer. At small angles, the MISO temperature dependence is controlled by variations of the electron quantum lifetime due to the temperature dependence of electron–electron scattering. At large angles $\theta$, the temperature damping of MISO amplitude increases and demonstrates an additional, exponentially strong decrease of the MISO magnitude with the temperature.[17]

A proposed model relates this additional MISO suppression to an entanglement between subbands, which is induced by the in-plane magnetic field. The magnetic entanglement leads to a difference in the electron cyclotron masses and, thus, to a misalignment between spectra in two subbands, which results in the suppression of MISO magnitude. For the free electron systems, the effect of the magnetic entanglement on the MISO magnitude is described by an universal MISO damping factor: $A_{MISO}(T) = X/\sinh(X)$, where $X = 2\pi^2 kT\delta f$ and $\delta f$ is the difference frequency of oscillations of density of states in two subbands.[17]

A comparison with the experiment demonstrates the adequacy of the model. In addition, the comparison reveals enhancement of the MISO magnitude. Surprisingly, this enhancement is found to be reasonably described by the Fermi-liquid theory, taking into account that the quantum lifetime of 2D electrons depends on the electron energy. Thus, the observed enhancement of MISO amplitude provides an access to the energy dependence of the electron quantum lifetime.

In this paper, we investigate the relation between observed enhancement of MISO amplitude and the energy dependence of the electron quantum lifetime within the Fermi-liquid theory. Using two different approaches, we extract the Fermi-liquid parameter, $\varepsilon_F^*$, which describes the energy dependent contributions of the electron–electron interaction to the quantum lifetime. We find that both methods yield consistent but not the identical results for both $\varepsilon_F^*$ and $df$. The results suggest also that the spin splitting of Landau levels is an important factor in the suppression of MISO magnitude.

## II. EXPERIMENTAL SETUP

Studied GaAs quantum wells were grown by molecular beam epitaxy on a semi-insulating (001) GaAs substrate. The material was fabricated from a selectively doped GaAs single quantum well of width $d = 26$ nm sandwiched between AlAs/GaAs superlattice screening barriers.[18–22] The studied samples were etched in the shape of a Hall bar. The width and the length of the measured part of the samples are $W = 50\,\mu$m and $L = 250\,\mu$m. AuGe eutectic was used to provide electric contacts to the 2D electron gas. Samples were studied at different temperatures, from 5.5 to 12 K in magnetic fields up to 7 T applied at different angle $\theta$ relative to the normal to 2D layers and perpendicular to the applied current. The angle $\theta$ is evaluated using Hall voltage $V_H = B_\perp/(en_T)$, which is proportional to the perpendicular component, $B_\perp = B\cos(\theta)$, of the total magnetic field **B**.

The total electron density of sample S1, $n_T = (8.0 \pm 0.03) \times 10^{11}\,\mathrm{cm}^{-2}$, was evaluated from the Hall measurements taken in classically strong magnetic fields.[2] An average electron mobility $\mu \approx 72\,\mathrm{m}^2/\mathrm{Vs}$ was obtained from $n_T$ and the zero-field resistivity. An analysis of the periodicity of MISO in the inverse magnetic field yields the gap $\Delta_{12} = 15.15$ meV between bottoms of the conducting subbands, Fermi energy $E_F = 21.83$ meV, and electron densities $n_1 = 6.12 \times 10^{11}\,\mathrm{cm}^{-2}$ and $n_2 = 1.87 \times 10^{11}\,\mathrm{cm}^{-2}$ in the two populated subbands. Sample S2 has density $n_T \approx 8.66 \times 10^{11}\,\mathrm{cm}^{-2}$, mobility $\mu \approx 96.5 \times \mathrm{m}^2/\mathrm{Vs}$, the gap $\Delta_{12} = 16$ meV, Fermi energy $E_F = 23.5$ meV and electron densities $n_1 = 6.57 \times 10^{11}\,\mathrm{cm}^{-2}$ and $n_2 = 2.09 \times 10^{11}\,\mathrm{cm}^{-2}$. Both samples have demonstrated similar behavior in magnetic fields.

Sample resistance was measured using the four-point probe method. We applied 133 Hz *ac* excitation $I_{ac} = 1\,\mu$A through the current contacts and measured the longitudinal (in the direction of the electric current, *x*-direction) and Hall *ac* (along *y*-direction) voltages ($V_{xx}^{ac}$ and $V_H^{ac}$) using two lock-in amplifiers with 10 MΩ input impedance. The measurements were done in the linear regime in which the voltages are proportional to the applied current.

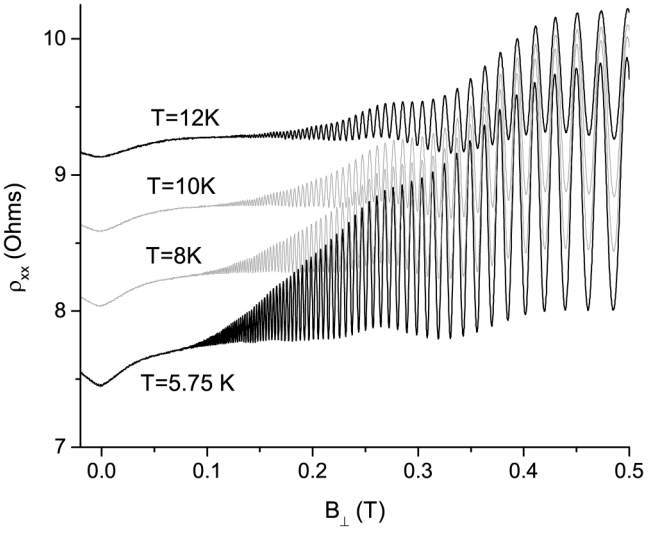


**FIG. 1.** Dependencies of the dissipative resistivity of 2D electrons, $\rho_{xx}$, on the perpendicular magnetic field taken at different temperatures as labeled. Angle $\theta = 0°$. Sample S2.

## III. EXPERIMENTAL RESULTS

Figure 1 shows dependencies of the dissipative resistivity of 2D electrons on the perpendicular magnetic field $B_\perp$, taken at different temperatures T and the angle $\theta = 0^0$ between the direction of the magnetic field **B** and the normal to the 2D layer. At $\theta = 0^0$, two subbands are disentangled. At small magnetic fields ($B_\perp < 0.05$ T), the curves demonstrate an increase related to the classical magnetoresistivity.[2,16] At higher magnetic fields, $B_\perp > 0.08$ T, the resistivity starts to oscillate with a progressively larger magnitude at higher fields. These are MIS-oscillations. MISO maxima correspond to the condition

$$E_g = k\hbar\omega_c, \tag{1}$$

where $E_g = E_2 - E_1$ is the energy difference between bottoms of two occupied subbands and the index $k$ is a positive integer.[13,15]

The temperature significantly affects the MISO magnitude. At temperature $T = 12$ K, the MISO magnitude is substantially smaller than the one at $T = 5.75$ K. Furthermore, at a higher temperature, the MIS-oscillations start at a higher magnetic field. Both effects result from an increase of the quantum scattering rate of electrons at a higher temperature due to the enhancement of electron–electron scattering.[8,9,23] This rate enters the Dingle factor, affecting strongly

MISO magnitude [see Eq. (6)]. The experiment indicates that the Hall resistivity and, thus, the total electron density in the system are not affected by the temperature (not shown).

To facilitate the analysis of the oscillating content, the monotonic background $\rho^b_{xx}$, obtained by averaging of the oscillations in reciprocal perpendicular magnetic fields, is removed from the magnetoresistivity $\rho_{xx}(B_\perp)$. Figure 2 presents the remaining oscillating content of the magnetoresistivity, $\rho_{MISO} = \rho_{xx} - \rho^b_{xx}$, as a function of the reciprocal perpendicular magnetic field $B_\perp^{-1}$ for two temperatures as labeled. The thin solid lines indicate envelopes of the oscillations used in the analysis below.

In Fig. 2, panel (a) presents data taken at angle $\theta = 0^\circ$ and corresponding to disentangled subbands. Panel (a) demonstrates that at a high temperature $T = 12$ K, the MISO magnitude is smaller than the one at $T = 5.75$ K. An analysis of the MISO envelope indicates that the MISO magnitude decreases exponentially with $1/B_\perp$ at a small $1/B_\perp$. The rate of the exponential decrease is stronger at the higher temperature. Both the thermal suppression of MISO and the increase of the MISO decay with $1/B_\perp$ are a result of the increase of the quantum scattering rate of 2D electrons, $1/\tau_q$, due to the increase of electron–electron scattering at high temperatures.

In Fig. 2, panel (b) demonstrates the dependence of MISO on $1/B_\perp$ for the magnetically entangled subbands at $\theta = 85.7^\circ$. The decrease of MISO magnitude with $1/B_\perp$ is different from the exponential decrease of the disentangled subbands. The magnetic field dependence tends to saturate at small $1/B_\perp$ in contrast to the one shown in panel (a). For the entangled subbands, the MISO magnitude is significantly reduced. Furthermore, rough analysis indicates that the relative decrease of the MISO magnitude with the temperature is substantially stronger than the one for disentangled subbands. In particular, at $1/B_\perp = 3$ (1/T) for the disentangled subbands, the ratio between MISO magnitudes at $T_1 = 5.75$ K and $T_2 = 12$ K is close to 3, while for the entangled subbands, this ratio is larger and close to 10.[17]

Figure 3 presents the ratio of MISO magnitude of magnetically entangled subbands, obtained at angle $\theta = 85.7^\circ$ to the MISO magnitude of disentangled subbands at $\theta = 0^\circ$. This ratio is used to extract the Fermi-liquid parameter $\varepsilon_F^*$. Below we recall the model describing MIS-oscillations in magnetically entangled subbands.[17]

## IV. MODEL OF MISO IN MAGNETICALLY ENTANGLED SUBBANDS

We consider a 2D electron system with two populated parabolic subbands placed in a small quantizing perpendicular magnetic field $B_\perp$ and an in-plane magnetic field $B_\parallel$: $\mathbf{B} = (B_\perp, B_\parallel)$. At $B_\parallel = 0$ T, the cyclotron masses in two subbands are the same, $m_{c1} = m_{c2} = m_0$, and an application of the perpendicular magnetic field $B_\perp$ leads to equidistant Landau levels with separation $\hbar\omega_{c0} = \hbar eB_\perp/m_0$ in both subbands. Due to the energy gap between the bottoms of the subbands, $\Delta_{12}$, the Landau levels in the second subband are shifted up by $\Delta_{12}$ with respect to the energy levels in the first subband. At the condition, corresponding to Eq. (1), two sets of the levels are aligned with each other, producing a MISO maximum.

An application of the in-plane magnetic field destroys the alignment.[16,17] In accordance with numerical analysis of the electron spectrum, a non-zero in-plane magnetic field, $B_\parallel$, makes the cyclotron masses, $m_{c1} > m_{c2}$, and the cyclotron frequencies, $\omega_{c1} < \omega_{c2}$, to be different.[17] This difference leads to beating in the density of states (DOS), oscillating at different frequencies, $f_i$, in different subbands: $f_i = 1/\hbar\omega_{ci}$, where index $i = 1(2)$ corresponds to the first (second) subband.

At small quantizing magnetic fields $\omega_{ci}\tau_q < 1$, the main contribution to MISO comes from the fundamental harmonics of DOS

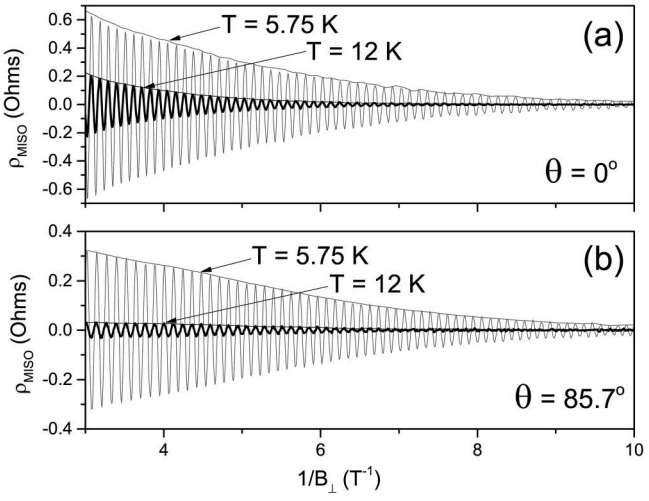


**FIG. 2.** Oscillating content of magnetoresistivity $\rho_{xx}$ at two different temperatures as labeled. (a) Disentangled subbands at angle $\theta = 0^\circ$ and (b) entangled subbands at angle $\theta = 85.7^\circ$. Sample S2.

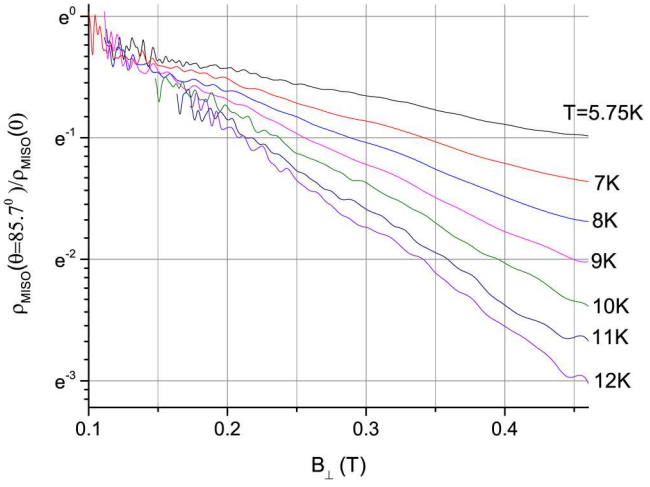


**FIG. 3.** Magnetic field dependence of the ratio $= \rho_{MISO}(\theta = 85.7^\circ)/\rho_{MISO}(\theta = 0^\circ)$ between the MISO amplitude in magnetically entangled subbands at $\theta = 85.7^\circ$ to the one in disentangled subbands at $\theta = 0^\circ$ ($B_\parallel = 0$ T) at different temperatures as labeled. Sample S2.

oscillations. The DOS of the $i$th spatial subband, $\nu_i(\varepsilon)$, reads[3,24]

$$\begin{aligned}\frac{\nu_1(\varepsilon\geq 0)}{\nu_{01}} &= 1-2\delta_1\cos(2\pi f_1\varepsilon),\\ \frac{\nu_2(\varepsilon\geq E_g)}{\nu_{02}} &= 1-2\delta_2\cos(2\pi f_2(\varepsilon-E_g)),\end{aligned} \tag{2}$$

where $\nu_{0i}$ represents DOS at zero perpendicular magnetic field, $\delta_i = exp(-\pi/\omega_{ci}\tau_q^{(i)})$ is the Dingle factor, and $\tau_q^{(i)}$ is the quantum scattering time in $i$th subbands. The parameters $\nu_{0i}$ describe DOS in the $kT$ vicinity of the Fermi energy. Within the $kT$ interval, the energy dependence of these parameters in a weakly non-parabolic spectrum of 2D electrons, induced by the in-plane magnetic field, is neglected. The parameter $E_g$ is the energy gap between bottoms of two subbands.

The 2D conductivity $\sigma$ is obtained from the following relation:

$$\sigma(\mathbf{B}) = \int d\varepsilon\sigma(\varepsilon)\left(-\frac{\partial f_T}{\partial\varepsilon}\right) = \langle\sigma(\varepsilon)\rangle. \tag{3}$$

The integral is an average of the conductivity $\sigma(\varepsilon)$ taken essentially for energies $\varepsilon$ inside the temperature interval $kT$ near Fermi energy, where $f_T(\varepsilon)$ is the electron distribution function at a temperature $T$.[2,3] The brackets $\langle\cdots\rangle$ represent this integral below. We consider the regime of high temperatures: $f_ikT \gg 1$. In this regime, Shubnikov–de Haas oscillations are suppressed, but MISO survive.

The conductivity $\sigma(\varepsilon)$ is proportional to square of the total density of states: $\sigma(\varepsilon) \sim (\nu_1(\varepsilon)+\nu_2(\varepsilon))^2$.[24,25] This relation yields the following term leading to MISO at small quantizing magnetic fields:[13,15]

$$\sigma_{MISO}(\varepsilon) = \sigma_D^{(12)}\tilde{\nu}_1(\varepsilon)\tilde{\nu}_2(\varepsilon), \tag{4}$$

where $\tilde{\nu}_i(\varepsilon) = \nu_i(\varepsilon)/\nu_{0i}$ are the normalized density of states in each spatial subband. The parameter $\sigma_D^{(12)}(B_\perp)$ is Drude like conductivity, accounting for inter-subband scattering.[13,15]

A substitution of Eqs. (4) and (2) into Eq. (3) yields the following expression for the MISO of conductivity:

$$\sigma_{MISO}(\mathbf{B}) = 4\sigma_D^{(12)}\delta_1\delta_2\langle\cos(2\pi f_1\varepsilon)\cos(2\pi f_2(\varepsilon-E_g))\rangle. \tag{5}$$

Energy integration yields the final result,[17]

$$\sigma_{MISO}(\mathbf{B}) = 2\sigma_D^{(12)}\delta_1\delta_2\frac{X}{\sinh(X)}\cos(2\pi f_2E_g + 2\pi\delta f\varepsilon_F), \tag{6}$$

where parameter $X = 2\pi^2kT\delta f$ and $\delta f = f_1 - f_2$ is a difference frequency.

Entangled subbands $\delta f > 0$ and the temperature damping factor $A_{MISO}(T) = X/\sinh(X)$ decrease the MISO amplitude. This temperature decrease becomes exponential for $X > 1$ since $\sinh(X) \sim \exp(X)$ for $X > 1$. The parameter $X$ is proportional to the temperature and the difference frequency $\delta f = f_1 - f_2$. Within the order of $B_\parallel^6$, the difference frequency is evaluated as

$$\delta f = \frac{m_0}{e\hbar}\chi(1-\xi B_\parallel^2+\eta B_\parallel^4)\tan^2(\theta)B_\perp, \tag{7}$$

where $\chi$, $\xi$, and $\eta$ are constants. The constants $\chi$ and $\xi$ are computed analytically for the magnetically entangled subbands.[17] Below, we use the relation (7) to compare experiments with the expression (6).

In many respects, the MISO temperature damping factor $A_{MISO}(T)$ is similar to the one for Shubnikov–de Haas oscillations, $A_{SdH}(T) = X_{SdH}/\sinh(X_{SdH})$, where $X_{SdH} = 2\pi^2kT/(\hbar\omega_{ci})$.[1] The main difference is that the factor $A_{MISO}$ depends on the difference frequency $\delta f$, whereas $A_{SdH}$ depends on the frequency $f_i = 1/\hbar\omega_{ci}$. For parabolic subbands with the same masses $\delta f = 0$ and the MISO damping factor $A_{MISO} = 1$ is irrelevant. The MISO damping factor is important for non-parabolic spectra or parabolic spectra with different cyclotron masses in two subbands.

Experimental data presented below suggest that in addition to the MISO temperature damping factor $A_{MISO}(T)$, there is an important effect of the electron–electron interaction on the MISO magnitude. To analyze this Fermi-liquid effect, we use several approaches.

## V. COMPARISON WITH THE EXPERIMENT

### A. Method 1

To reveal the temperature damping factor $A_{MISO}(X) = X/\sinh(X)$, we compare experimental data with the analytical expression (6) containing this factor. There are other factors ($\delta_i$, $\sigma_D^{(12)}$) entering the expression. A comparison with numerically computed MISO as well as analytical considerations indicate that the product of these factors varies weakly with the entanglement between subbands.[17] Below, we neglect these variations. To suppress effects of these factors in the comparison between Eq. (6) and experiment, for each temperature, we divide a MISO envelope for the entangled subbands, such as presented in Fig. 2(b) for T = 5.75 and T = 12 K, by the envelope for the disentangled subbands, taken at the same temperature presented in Fig. 2(a). This experimental ratio $R_{exp} = \rho_{MISO}(\theta)/\rho_{MISO}(0)$, shown in Fig. 3, is compared with the corresponding model ratio, $R_{mod} = \rho_{MISO}(\theta)/\rho_{MISO}(0) = \sigma_{MISO}(\theta)/\sigma_{MISO}(0)$ obtained from Eq. (6).

In accordance with Eq. (6) at $\tau_q^{(1)} = \tau_q^{(2)}$, the ratio of the MISO magnitudes $R_{mod} = X/\sinh(X)$ and depends only on the parameter $X$. Thus, plotted vs $X$, the ratio $R_{exp}(X)$ should follow $A_{MISO}(X) = X/\sinh(X)$. To facilitate the comparison at $X > 1$, both ratios are divided by $X$, yielding $y = R_{mod}/X \approx 2\exp(-X)$ at $X > 1$. At large X, the function $\ln(R_{mod}/X)$ vs $X$ is, thus, a straight line with a unity slope intersecting $y$-axis at $y_0 = 2$.

Experiments indicated that at large angles, the ratio $R_{exp}/X$ is indeed following an exponential reduction with parameter $X$ at a unity slope.[17] However, the ratio does not intersect the y axis exactly at $y_0 = 2$ but rather is distributed in its vicinity. Accounted below by a normalizing factor $K_{ee}$, these deviations depend on the angle $\theta$ and the temperature $T$. In method 1, the factor $K_{ee}$ normalizes the ratio $R_{exp}/X$ and makes each curve intersect the y-axis at value 2. The procedure leads to collapse of all experimental dependencies with the model dependence $1/\sinh(X)$. This collapse is presented in Fig. 4.

Figure 4 shows the ratio $R_{exp}/X$, normalized by factor $K_{ee}$, as a function of the parameter $X$ for dependencies $R_{exp} = \rho_{MISO}(\theta = 87.05°)/\rho_{MISO}(\theta = 0°)$ obtained for sample S1 at angle $\theta = 87.05°$ and temperatures T = 5.5, 6.14, 6.93, 7.74, 8.54, 9.34,

10.13, and 10.93 K (see Fig. 8 in Ref. 17). The parameter $X$ is computed from Eq. (7), using $\chi = 1.12 \times 10^{-5}\,[d(\text{nm})]^2$, $\xi = 1.91 \times 10^{-5}\,[d(\text{nm})]^2$, which are evaluated analytically,[17] and $\eta = 4 \times 10^{-10}\,[d(\text{nm})]^4$ found from the fit with the model. The presented comparison indicates a good agreement between the model and the experiment in a broad range of temperatures and magnetic fields.

The origin of the scaling coefficient $K_{ee}$ is related to effects of electron–electron interaction on the quantum scattering rate.[17] Within the Fermi-liquid theory, the electron–electron collision rate for an electron at energy $\varepsilon$ counted from the Fermi energy $\varepsilon_F$ is

$$\frac{1}{\tau_{ee}(\varepsilon, T)} = \frac{\varepsilon^2 + \pi^2 (kT)^2}{4\pi\hbar\varepsilon_F} \ln \frac{q_s v_F}{\max\left(kT, \hbar\omega_c(\omega_c\tau_{tr})^{1/2}\right)}, \tag{8}$$

where $v_F$ is the Fermi velocity, $\tau_{tr}$ is the transport scattering time, and $q_s = 2\pi e^2 \nu$ is the inversion screening length.[25,28]

The energy dependence of the electron scattering rate makes the Dingle factors $\delta_i$ to be energy dependent parameters,

$$\delta_i(\varepsilon, T) = \exp\left(-\frac{\tau_{im}^{-1} + \tau_{ee}^{-1}(\varepsilon, T)}{\omega_{ci}/\pi}\right), \tag{9}$$

where $\tau_{im}$ is the quantum scattering time due to impurity scattering. The time $\tau_{im}$ does not depend on the temperature, while the electron–electron scattering time $\tau_{ee}$ is temperature dependent. The time $\tau_{ee}$ provides the $T^2$ contribution to the quantum scattering rate observed in the experiments (see the inset to Fig. 7 in Ref. 17).

In the presented above computations of the ratio $R_{mod} = \sigma_{MISO}(\theta)/\sigma_{MISO}(0^0)$, the energy dependence of the Dingle factors $\delta_i$ in Eq. (6) was ignored canceling out these factors. The effect of the energy dependence of the $e-e$ scattering rate on the relative MISO magnitude: $R_{mod} = \rho_{MISO}(\theta)/\rho_{MISO}(0^0) = \sigma_{MISO}(\theta)/\sigma_{MISO}(0^0)$ is evaluated below. Substitution of the relations (4), (2), and (9) into Eq. (3) leads to the following expression for the relative MISO magnitude:

$$R_{mod} = \frac{\rho_{MISO}(\theta)}{\rho_{MISO}(0^0)} = \frac{\langle \exp(-\varepsilon^2/\varepsilon_0^2)\cos(2\pi\delta f\varepsilon)\rangle}{\langle \exp(-\varepsilon^2/\varepsilon_0^2)\rangle}, \tag{10}$$

where $\varepsilon_0 = (2\varepsilon_F^*\hbar\omega_c)^{1/2}$. In the estimation, a possible difference in the $e$–$e$ scattering rate in two subbands and the temperature/magnetic field dependencies of the logarithmic factor in Eq. (8) are ignored. As a result in Eq. (10), the only fitting parameter is $\varepsilon_F^* \sim \varepsilon_F^{(i)}/\ln\left(q_s v_F^{(i)}/\max\left(kT, \hbar\omega_c(\omega_c\tau_{tr})^{1/2}\right)\right)$ [see Eq. (8)]. The parameter $\varepsilon_F^*$ describes quantitatively the strength of the energy dependence of the electron quantum lifetime. It is extracted below from a comparison with the experiment. The energy dependence of the electron quantum lifetime is an important physical property of interacting electrons. The proportionality of the electron–electron scattering rate to $\varepsilon^2$ [see Eq. (8)] as well as its strength are the corner stone of the Fermi-liquid theory, describing interacting electron systems as a gas of quasiparticles.

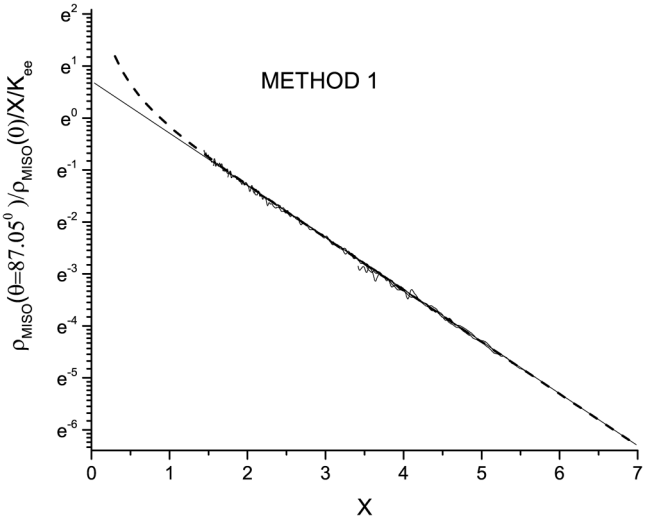


**FIG. 4.** Dependence of the ratio $R_{exp}$ of MISO magnitude, obtained at angle $\theta = 87.05°$ to the one at $\theta = 0°$ and normalized by $X$ and $K_{ee}$ on parameter $X$ at different temperatures $T$ = 5.5, 6.14, 6.93, 7.74, 8.54, 9.34, 10.13, and 10.9 K. The parameter $X$ is computed from Eq. (7), using $\chi = 1.12 \times 10^{-5}\,[d(\text{nm})]^2$, $\xi = 1.91 \times 10^{-5}\,[d(\text{nm})]^2$, evaluated analytically,[17] and $\eta = 4 \times 10^{-10}\,[d(\text{nm})]^4$, found from the fit with the model, at d = 26 nm. The dashed line presents the dependence 1/ sinh(X) expected from Eq. (6). The thin straight line presents the linear approximation of the dependence $\ln(R_{mod}/X) \approx \ln(2) - X$ with a unity slope and intersect $y_0 = 2$, expected from Eq. (6) at $X > 1$. Sample S1.

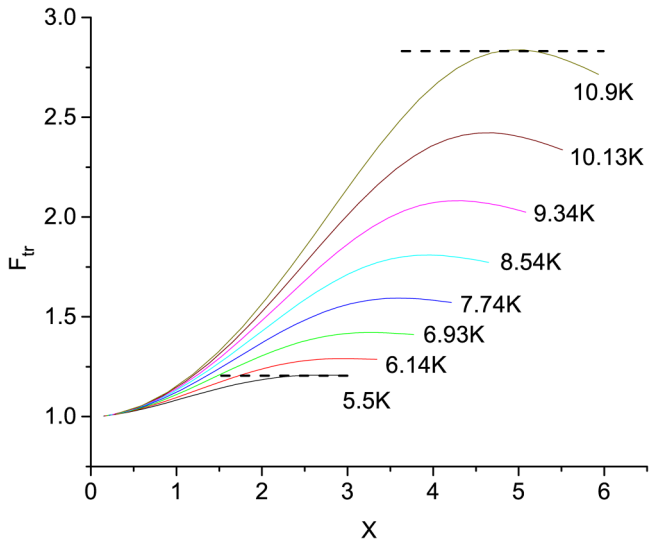


**FIG. 5.** Dependence of the transition function $F_{tr}$ on parameter $X$ at different temperatures as labeled. The function $F_{tr}$ is numerically computed from Eq. (11) at $\varepsilon_F^* = 8$ meV, using parameter $X$ evaluated numerically from Eq. (7) at $\chi = 1.12 \times 10^{-5}\,[d(\text{nm})]^2$, $\xi = 1.91 \times 10^{-5}\,[d(\text{nm})]^2$, $\eta = 4 \times 10^{-10}\,[d(\text{nm})]^4$, and d = 26 nm at angle $\theta = 87.05°$. Dashed lines show approximation of the transition function by a constant in the interval $X$ relevant to the experiment shown in Fig. 4.

A comparison with the free electron case suggests that the ratio $R_{mod}$ can be presented as a product of $X/\sinh(X)$, corresponding to free electrons, and a transition function $F_{tr}(X, \theta, T)$, describing an enhancement of the MISO magnitude by the electron–electron interaction,

$$R_{mod} = F_{tr}(X, \theta, T)\frac{X}{\sinh(X)}. \quad (11)$$

Figure 5 shows an example of the numerically evaluated function $F_{tr}(X, \theta, T)$ using the relation (11) at different temperature T as labeled. At a fixed temperature, the MISO enhancement (function $F_{tr}$) progresses with the parameter $X$. At $X < 1$, corresponding to a small entanglement between subbands, the function $F_{tr}$ tends to unity, and thus, the ratio $R_{mod}$ approaches the free electron response, $X/\sinh(X)$. At this condition, the MISO enhancement is small. At larger $X$, the MISO enhancement increases and eventually reaches a maximum. In the vicinity of the maximum, the transitional function $F_{tr}$ is approximated by a constant value. Dashed lines are examples of these approximations for $T = 5.5$ and 10.9 K demonstrating also the range of the parameters $X$ relevant to the experiments shown in Fig. 4. The approximation of the function $F_{tr}$ by a constant agrees with the unity slope of the experimental dependencies presented in Fig. 4 and yields the model scaling coefficient $K_{ee}^{mod}$. Within Method 1, this approximation is used to compare the experiment and the model.

Shown in Fig. 5 an increase of the function $F_{tr}(X, \theta, T)$ with $X$ from the unity at small $X$ to a temperature dependent maximum

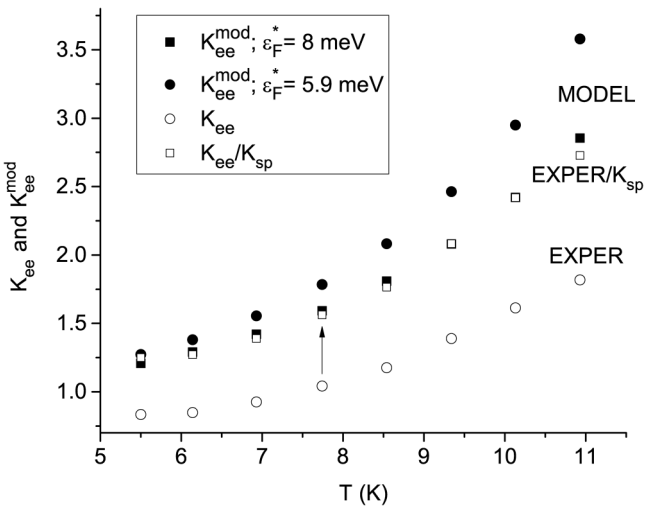


**FIG. 6.** Open circles present temperature dependence of scaling coefficient $K_{ee}$ obtained from a collapse of experimental data on a free electron response, shown in Fig. 4. Open squares present coefficient $K_{ee}$, normalized by spin factor $K_{sp} = 0.67$. Filled squares present temperature dependence of scaling coefficient $K_{ee}^{mod}$ evaluated numerically as shown in Fig. 5 at $\varepsilon_F^* = 8$ meV, providing the best fit within method 1. Filled circles present coefficient $K_{ee}^{mod}$ evaluated numerically as shown in Fig. 5 but at $\varepsilon_F^* = 5.9$ meV, which corresponds to the observed temperatures dependence of MISO amplitude (not shown). Angle $\theta = 87.05°$. Sample S1.

is a result of the electron–electron interaction and is a Fermi-liquid effect. The electron–electron interaction leads to a decrease of the quantum lifetime of quasiparticles with the energy $\varepsilon$ away from the Fermi energy.[26,27] Equations (8) and (9) take into account this lifetime reduction resulting in the Gaussian $\exp(-\varepsilon^2/\varepsilon_0^2)$ in Eq. (10). The Gaussian function enhances the MISO amplitude. Mathematically, the effect is due to a reduction of the range of the energy integration in Eq. (10) from $(-kT, kT)$, settled by the distribution function $f_T$ for free electrons, to a smaller range, which for the interacting electrons is additionally affected by the range narrowing factor $\exp(-\varepsilon^2/\varepsilon_0^2)$. The energy averaging of the oscillating content $[\cos(2\pi\delta f\varepsilon)]$ in a narrower energy interval leads to suppression of the averaging and results in a larger value of the integral and, thus, the function $F_{tr}(X, \theta, T)$.[28]

Figure 6 presents a comparison between the experiment and the model using Method 1. In Fig. 6, the open circles present the scaling coefficient, $K_{ee}$, obtained via the collapse of the experimental data on the free electron result shown in Fig. 4. The filled circles and squares present a result of the numerical computations of the transition function $F_{tr}$ at $\varepsilon_F^* = 5.9$ meV and $\varepsilon_F^* = 8$ meV and subsequent approximation of the function by constant $K_{ee}^{mod}$ as shown in Fig. 5. The numerical computations indicate that the Fermi-liquid enhancement of the MISO magnitude is stronger at smaller $\varepsilon_F^*$. This is related to a narrower Gaussian function in Eq. (10) at smaller $\varepsilon_F^*$, leading to smaller $\varepsilon_0$.

Figure 6 indicates that similar to the numerically obtained $K_{ee}^{mod}$, the scaling coefficient $K_{ee}$ increases with the temperatures. However, at low temperature $T = 5.5$ K, in contrast to $K_{ee}^{mod}$, the coefficient $K_{ee}$ is less than unity. This property progresses with the increasing angle and is consistent for all studied samples. This property suggests the presence of an angular dependent factor, reducing additionally the MISO magnitude in magnetic fields. We related this factor to spin splitting of Landau levels.

For SdH oscillations, the spin splitting decreases the oscillation magnitude for angles less than a critical angle.[3] The reduction is a result of the decrease of the magnitude of the DOS oscillations with the spin splitting of Landau levels. Recently, we have observed a reduction of the magnitude of the quantum positive magnetoresistance (QPMR)[24] and MISO[16] at large angles $\theta$. For QPMR, the spin splitting is found to be the dominant mechanism leading to the decrease of the magnetoresistance. The spin splitting also leads to MISO reduction but is found to be a subdominant effect in comparison with the effect of the magnetic entanglement of subbands presented above. For MISO, the spin factor reads[16]

$$K_{sp} = \cos^2\left(\frac{\pi\Delta_Z}{\hbar\omega_c}\right), \quad (12)$$

where $\Delta_Z = \mu g B$ is the Zeeman energy, $\mu$ is the Bohr magneton, and $g$ is the g-factor. In the relation (12), we assume that the Zeeman splitting in both subbands is the same. The ratio $\Delta_Z/(\hbar\omega_c) \sim g/\cos(\theta)$ and, thus, the spin factor $K_{sp}$ depend on $g$ and the angle $\theta$. For experiments at a fixed angle, the spin factor is a constant affecting the ratio $R_{exp}$: $R_{exp} = (K_{sp}(\theta)/K_{sp}(0))R_{mod} \approx K_{sp}(\theta)R_{mod}$ since for GaAs at $g \sim 1$ and $\theta = 0$ deg, the spin factor is close to one: $K_{sp}(\theta = 0) \approx 1$.

To find the spin factor, we divide the scaling coefficient $K_{ee}$, describing $R_{exp}$, by the $K_{sp}$ to find the best fit with $K_{ee}^{mod}$, describing $R_{mod}$ computed from Eq. (10) at a $\varepsilon_F^*$. An example of the fit is shown in Fig. 6: the normalized experimental data, labeled by $EXPER/K_{sp}$, correlate well with the model computations $K_{ee}^{mod}$ at $\varepsilon_F^* = 8$ meV.

The obtained spin factor $K_{sp} = 0.67$ yields $g$-factor $g \approx 0.3$. This factor is in agreement with the one obtained before.[16] Other angles and samples demonstrate spin factors, which are consistent with Eq. (12) at $g \approx 0.2 - 0.4$. In Fig. 7, open symbols present the spin factors obtained at different angles $\theta$, while the solid line presents the computation of the spin factor in accordance with Eq. (12), using g-factor $g = 0.31$. We note that the obtained g-factor is close to the bare g-factor $g = 0.4$ in GaAs but is considerably smaller than the one obtained from the angular dependence of SdH oscillations and QPMR in GaAs quantum wells with only single band populated ($g \approx 1$).[24]

In accordance with Eq. (8), the temperature and the energy dependencies of the $e$–$e$ scattering rate are controlled by the same parameter $\varepsilon_F^*$. This should lead to a correlation between Fermi-liquid enhancement of the MISO amplitude and the temperature dependence of MISO. The temperature dependence yields $\varepsilon_F^* = 5.9$ meV.[17] Shown in Fig. 6 the model evaluation of $K_{ee}^{mod}$ at $\varepsilon_F^* = 5$ demonstrates MISO enhancement, which is quite comparable but still stronger than the one obtained in the experiments.

### B. Method 2

One of the disadvantages of method 1 is the requirement to compute parameter $X$ using a model for the difference frequency $df$. Within a given shape of the quantum well, the computations (numerical or analytical) of the difference frequency are possible. However, if the shape of the quantum well is not well known, the computation of the difference frequency presents a challenge. Thus, it is beneficial to develop a method in which the computation of the difference frequency is not required. Below, we present such a method and call it method 2.

The main idea of method 2 is to use the same ratio $R_{exp} = \rho_{MISO}(\theta)/\rho_{MISO}(0)(\mathbf{B}, T)$ but, in contrast to method 1, to use this ratio at a fixed magnetic field $\mathbf{B}$. At a fixed magnetic field, the entanglement between subbands and, thus, the difference frequency $df$ is also fixed. This allows one to consider the difference frequency as a fitting parameter and to obtain its value from the fit.

Figure 8 presents the fit using method 2. In the figure, open circles present the ratio $R_{exp} = \rho_{MISO}(\theta)/\rho_{MISO}(0)$ obtained at a fixed magnetic field. The perpendicular component of the field labels each experimental set. Each data set is obtained from a vertical cross section of the dependencies $R_{exp}(\mathbf{B})$ plotted vs $B_\perp$ at different temperatures similar to the plot shown in Fig. 3. The solid lines present computations of the ratio $R_{mod}$ using Eq. (10) with $df$ and $\varepsilon_F^*$ as two fitting parameters. The fit is done neglecting the spin splitting at $K_{sp}$=1. The obtained fitting parameters $df$ and $\varepsilon_F^*$ are shown by open circles in Figs. 10 and 11 correspondingly. Values of the difference frequency $df$ are found to be consistently higher than the one obtained from the numerical computations for a rectangular quantum well and shown by the dashed line in Fig. 10. Variations of both $df$s with $B_\parallel$ look quite similar. In Fig. 11, values of the parameter $\varepsilon_F^*$ at $K_{sp} = 1$ are found to be considerably smaller than the one obtained via method 1 at

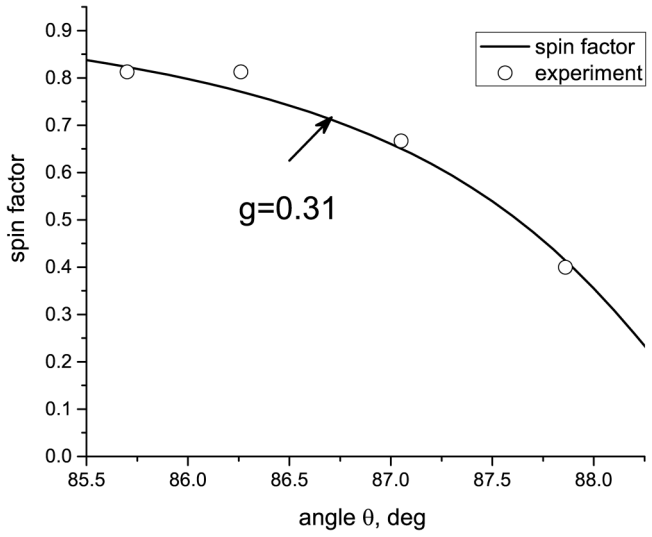


**FIG. 7.** Angular dependence of spin factor $K_{sp}$. Open symbols present spin factor $K_{sp}$ extracted from the comparison between the enhancement of the MISO amplitude and the model presented in Fig. 6 for $\theta = 87.05$ deg. The solid line shows spin factor $K_{sp}$ following from relation (12) using g-factor $g = 0.31$.

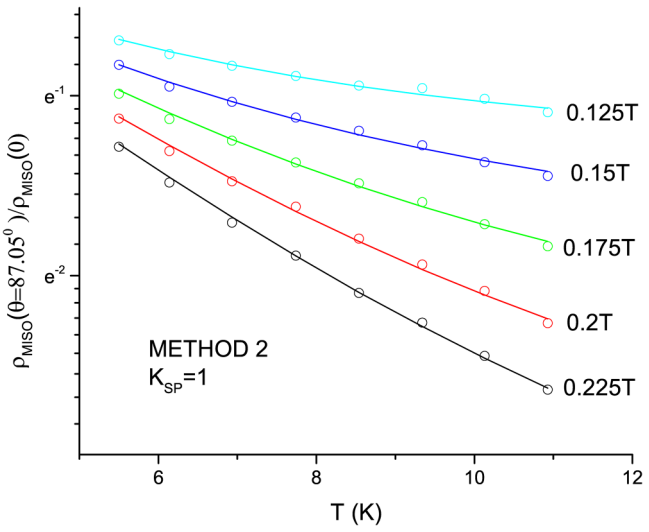


**FIG. 8.** Temperature dependence of ratio $\rho_{MISO}(\theta)/\rho_{MISO}(0)$ at different perpendicular magnetic fields as labeled. Open circles present experimental data. Solid lines present computation of the ratio $R_{mod}$, using Eq. (10) with $df$ and $\varepsilon_F^*$ as fitting parameters. Spin splitting is neglected: $K_{sp} = 1$. Angle $\theta = 87.05°$. Sample S1.

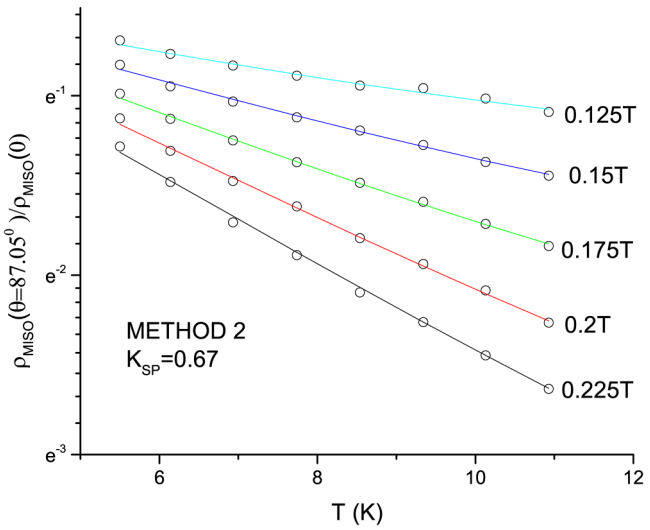


**FIG. 9.** Temperature dependence of ratio $\rho_{MISO}(\theta)/\rho_{MISO}(0)$ at different perpendicular magnetic fields as labeled. Open circles present experimental data. Solid lines present computation of the product $R_{mod}K_{sp}$ using Eq. (10) with $df$ and $\varepsilon_F^*$ as fitting parameters. Spin splitting factor $K_{sp} = 0.67$. Angle $\theta = 87.05°$. Sample S1.

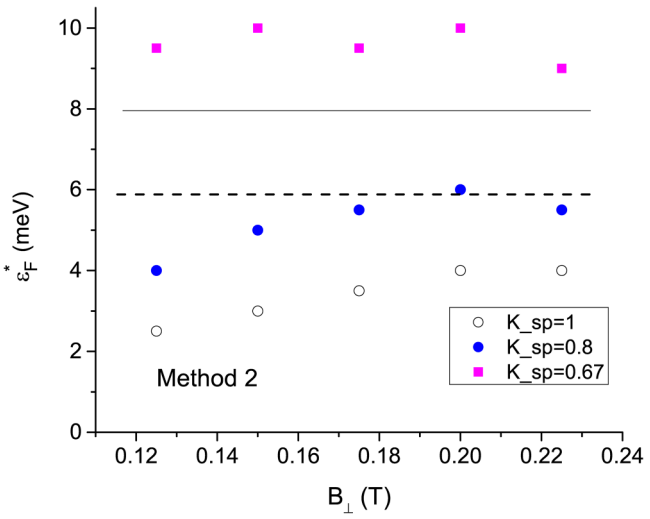


**FIG. 11.** Magnetic field dependence of the parameter $\varepsilon_F^*$. Open (filled) circles present $\varepsilon_F^*$ obtained in the fit using method 2 at $K_{sp} = 1$(=0.8). Filled squares present $\varepsilon_F^*$ obtained in the fit using method 2 at $K_{sp} = 0.67$. The solid line indicates $\varepsilon_F^* = 8$ meV obtained in the fit using method 1. The dashed line indicates $\varepsilon_F^* = 5.9$ meV obtained from the temperature dependence of MISO amplitude.

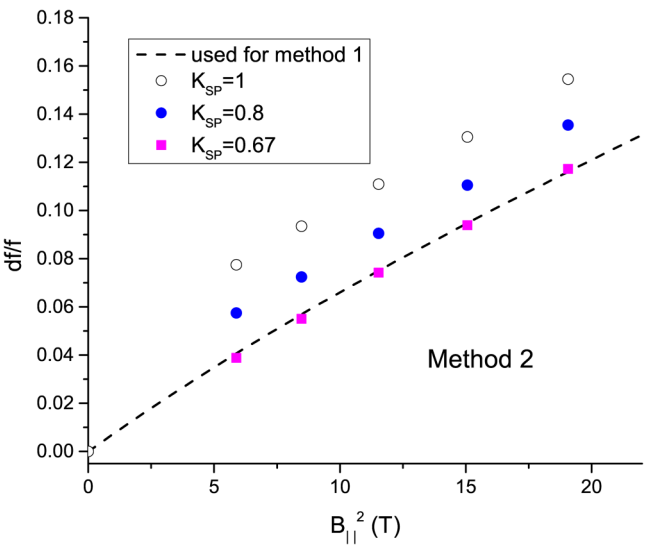


**FIG. 10.** Dependence of relative difference frequency, $df/f$, on the square of the in-plane magnetic field. The dashed line presents $df/f$, numerically computed for a rectangular quantum well using Eq. (7) at $\chi = 1.12 \times 10^{-5}$ [$d$(nm)]$^2$, $\xi = 1.91 \times 10^{-5}$ [$d$(nm)]$^2$, $\eta = 4 \times 10^{-10}$ [$d$(nm)]$^4$ and d = 26 nm. Open (filled) circles present $df/f$ obtained in the fit using method 2 at $K_{sp} = 1$ (=0.8). Filled squares present $df/f$, obtained in the fit at $K_{sp} = 0.67$. Angle $\theta = 87.05°$. Sample S1.

$\varepsilon_F^* = 8$ meV and demonstrate a tendency to increase from 2 to 4 meV with the increase in the magnetic field.

Figure 9 presents the fit using method 2 at spin splitting $K_{sp} = 0.67$. In the figure, open circles present the same ratio $R_{exp} = \rho_{MISO}(\theta)/\rho_{MISO}(0)$ as in Fig. 8. The solid lines present computations of the product $R_{mod}K_{sp}$ using Eq. (10) with $df$ and $\varepsilon_F^*$ as two fitting parameters. The accuracy of this fit is quite comparable with the accuracy of the fit at $K_{sp} = 1$. Obtained in this fit values of $df$ and $\varepsilon_F^*$ are shown by filled squares in Figs. 10 and 11 correspondingly. The values for the difference frequency $df/f$ are found to be almost identical to the difference frequency $df/f$, used in method 1 and shown by the dashed line in Fig. 10. In Fig. 11, the filled squares, presenting the parameter $\varepsilon_F^*$, are slightly higher than the value of $\varepsilon_F^*$ found in method 1 (8 meV) and shown by the solid line in Fig. 11.

Finally, in Figs. 10 and 11, filled circles present fitting parameters $df$ and $\varepsilon_F^*$ obtained in the fit using method 2 at $K_{sp} = 0.8$. The data, shown in these figures, indicate a consistent decrease (increase) of the fitting parameter $df$ ($\varepsilon_F^*$) with the decrease of the spin factor $K_{sp}$. It leads to an uncertainty of the obtained fitting parameters in method 2.

## VI. SUMMARY

Electron–electron interaction induced enhancement of the amplitude of magneto-intersubband quantum oscillations of dissipative resistivity is observed in GaAs quantum wells with two populated subbands, placed in tilted magnetic fields at different temperatures $T$. The enhancement is related to a progressive decrease of the quantum lifetime of electrons with the energy away from the Fermi energy. The effect is studied by two methods,

yielding effective energy parameter, $\varepsilon_F^*$, controlling the energy dependence of the quantum electron lifetime, and the difference frequency, $df = f_1 - f_2$, of DOS oscillations with frequency $f_1$ and $f_2$ in two subbands.

In method 1, the difference frequency is computed within a model of a rectangular quantum well of width $d$. The energy parameter, $\varepsilon_F^*$, is obtained, then, as a fitting parameter in a comparison between the experiment and the proposed MISO model, taking into account the energy dependence of the quantum electron lifetime within Fermi-liquid theory. A good agreement is found between the experiment and the model in a broad range of magnetic fields and temperatures. The obtained value of the parameter $\varepsilon_F^* = 8$ meV is found to be quite close to the one obtained from the temperature dependence of the MISO amplitude $\varepsilon_F^* = 5.9$ meV. This correlation is expected within the existing theory, describing quantum lifetime of interacting electrons. Within method 1, the comparison between the experiment and the model indicates also the presence of an additional factor, reducing the MISO amplitude. This factor is related to spin splitting of the Landau levels and yields the $g$-factor: $g \approx 0.3$. This $g$-factor value is close to the one obtained in other experiments in two subband systems.

In method 2, the energy parameter, $\varepsilon_F^*$, and the difference frequency, $df$, are considered two fitting parameters in the comparison between the experiment and the model. The comparison is done for data sets obtained at a fixed magnetic field and different temperatures for different values of the spin splitting characterized by spin factor $K_{sp}$. At $K_{sp} = 1$, corresponding to the absence of the spit splitting, method 2 yields $\varepsilon_F^*$ varying from 2 to 4 meV. These values are smaller than the one obtained both in method 1 and via temperature dependence of the MISO amplitude. At $K_{sp} = 1$, the relative difference frequency $df/f$ is found to be consistently larger than the one obtained in method 1. The frequency demonstrates the same variations with the in-plane magnetic field. The considerable deviations between outputs of method 1 and method 2 suggest the importance of the spin factor.

At $K_{sp} = 0.67$, the obtained relative difference frequency $df/f$ is almost the same as the one used in method 1. The parameter $\varepsilon_F^*$ is found to be quite close but not identical to the one obtained in method 1. This parameter $\varepsilon_F^*$ is larger than the one obtained via temperature dependence of the MISO amplitude. These inconsistencies call for further improvements of the used approaches.

## ACKNOWLEDGMENTS

This work was supported by the National Science Foundation (Division of Material Research No. 1702594) and by the Russian Foundation for Basic Research (Project No. 20-02-00309).

## AUTHOR DECLARATIONS

### Conflict of Interest

The authors have no conflicts to disclose.

### Author Contributions

**Sara Abedi:** Data curation (equal); Investigation (equal); Software (equal); Writing – original draft (equal); Writing – review & editing (equal). **Sergey Vitkalov:** Funding acquisition (lead); Investigation (equal); Project administration (lead); Writing – original draft (equal); Writing – review & editing (equal). **A. A. Bykov:** Funding acquisition (equal); Investigation (equal); Project administration (equal); Writing – original draft (equal). **A. K. Bakarov:** Funding acquisition (equal); Investigation (equal); Resources (equal).

## DATA AVAILABILITY

The data that support the findings of this study are available from the corresponding author upon reasonable request.

## REFERENCES

[1]D. Shoenberg, *Magnetic Oscillations in Metals* (Cambridge University Press, New York, 1984).
[2]J. M. Ziman, *Principles of the Theory of Solids* (Cambridge University Press, 1972).
[3]T. Ando, A. B. Fowler, and F. Stern, Rev. Mod. Phys. B **54**, 437 (1982).
[4]S. D. Sarma and A. Pinczuk, *Perspectives in Quantum Hall Effects* (Wiley-VCH, Weinheim, 2004).
[5]P. T. Coleridge, Semicond. Sci. Technol. **5**, 961 (1990).
[6]D. R. Leadley, R. Fletcher, R. J. Nicholas, F. Tao, C. T. Foxon, and J. J. Harris, Phys. Rev. B **46**, 12439 (1992).
[7]A. Bykov, D. R. Islamov, A. V. Goran, and A. I. Toropov, JETP Lett. **87**, 477 (2008).
[8]N. C. Mamani, G. M. Gusev, T. E. Lamas, A. K. Bakarov, and O. E. Raichev, Phys. Rev. B **77**, 205327 (2008).
[9]A. V. Goran, A. A. Bykov, A. I. Toropov, and S. A. Vitkalov, Phys. Rev. B **80**, 193305 (2009).
[10]A. A. Bykov, A. V. Goran, and S. A. Vitkalov, Phys. Rev. B **81**, 155322 (2010).
[11]L. I. Magarill and A. A. Romanov, Fiz. Tverd. Tela **13**, 993 (1971). [Sov. Phys.-Solid State **13**, 828 (1971)].
[12]V. M. Polyanovskii, Fiz. Tekh. Poluprovodn. **22**, 2230 (1988). [Sov. Phys.-Semicond. **22**, 1408 (1988)].
[13]M. E. Raikh and T. V. Shahbazyan, Phys. Rev. B **49**, 5531 (1994).
[14]N. S. Averkiev, L. E. Golub, S. A. Tarasenko, and M. Willander, J. Phys.: Condens. Matter **13**, 2517 (2001).
[15]O. E. Raichev, Phys. Rev. B **78**, 125304 (2008).
[16]W. Mayer, S. Vitkalov, and A. A. Bykov, Phys. Rev. B **96**, 045436 (2017).
[17]S. Abedi, S. A. Vitkalov, A. A. Bykov, and A. K. Bakarov, Phys. Rev. B **104**, 075416 (2021).
[18]K.-J. Friedland, R. Hey, H. Kostial, R. Klann, and K. Ploog, Phys. Rev. Lett. **77**, 4616 (1996).
[19]D. V. Dmitriev, I. S. Strygin, A. A. Bykov, S. Dietrich, and S. A. Vitkalov, JETP Lett. **95**, 420 (2012).
[20]J. Kanter, S. Vitkalov, and A. A. Bykov, Phys. Rev. B **97**, 205440 (2018).
[21]M. Sammon, M. A. Zudov, and B. I. Shklovskii, Phys. Rev. Mater. **2**, 064604 (2018).
[22]T. Akiho and K. Muraki, Phys. Rev. Appl. **15**, 024003 (2021).
[23]S. Dietrich, S. Vitkalov, D. V. Dmitriev, and A. A. Bykov, Phys. Rev. B **85**, 115312 (2012).
[24]W. Mayer, A. Ghazaryan, P. Ghaemi, S. Vitkalov, and A. A. Bykov, Phys. Rev. B **94**, 195312 (2016).
[25]I. A. Dmitriev, M. G. Vavilov, I. L. Aleiner, A. D. Mirlin, and D. G. Polyakov, Phys. Rev. B **71**, 115316 (2005).
[26]G. W. Martin, D. L. Maslov, and M. Y. Reizer, Phys. Rev. B **68**, 241309(R) (2003).
[27]Y. Adamov, I. V. Gornyi, and A. D. Mirlin, Phys. Rev. B **73**, 045426 (2006).
[28]I. A. Dmitriev, M. Khodas, A. D. Mirlin, D. G. Polyakov, and M. G. Vavilov, Phys. Rev. B **80**, 165327 (2009).